

Generalized Loschmidt echo and information scrambling in open systems

Yi-Neng Zhou^{1,2,*} and Chang Liu^{1,3,†}

¹*Institute for Advanced Study, Tsinghua University, Beijing, 100084, China*

²*Department of Theoretical Physics, University of Genève, 1211 Genève 4, Suisse*

³*Department of Physics, National University of Singapore, Singapore 117542*

(Dated: December 4, 2024)

Quantum information scrambling, typically explored in closed quantum systems, describes the spread of initially localized information throughout a system and can be quantified by measures such as the Loschmidt echo (LE) and out-of-time-order correlator (OTOC). In this paper, we explore information scrambling in the presence of dissipation by generalizing the concepts of LE and OTOC to open quantum systems governed by Lindblad dynamics. We investigate the universal dynamics of the generalized LE across regimes of weak and strong dissipation. In the weak dissipation regime, we identify a universal structure, while in the strong dissipation regime, we observe a distinctive two-local-minima structure, which we interpret through an analysis of the Lindblad spectrum. Furthermore, we establish connections between the thermal averages of LE and OTOC and prove a general relation between OTOC and Rényi entropy in open systems. Finally, we propose an experimental protocol for measuring OTOC in open systems. These findings provide deeper insights into information scrambling under dissipation and pave the way for experimental studies in open quantum systems.

I. INTRODUCTION

Quantum information scrambling has become a pivotal concept in understanding the dynamics of quantum many-body systems, attracting significant attention in recent years. In closed quantum systems, it describes the process by which initially localized quantum information spreads throughout the system, rendering it inaccessible to local measurements. This phenomenon is closely tied to the thermalization dynamics of many-body systems and serves as a key diagnostic for quantum chaos.

One of the most prominent tools for probing quantum information scrambling is the out-of-time-order correlator (OTOC) [1, 2], which has been extensively studied across various areas of physics [3–27] and has recently been measured in experiments [28–36]. Another quantity closely related to the dynamics of information scrambling is the Loschmidt echo (LE) [37–42], which characterizes the retrieval fidelity of a quantum state after an imperfect time-reversal procedure, and has also been measured in experiments [43–53]. The LE reveals that even small perturbations in the Hamiltonian can lead to significant changes in the system’s dynamics, a hallmark of quantum chaotic behavior.

In closed quantum systems, information scrambling has been extensively studied, with general relations between quantities such as the LE and the OTOC being widely explored [53–66]. However, in realistic experimental settings, interactions between the system and its environment are unavoidable. The presence of dissipation and decoherence significantly modifies the universal behavior of information scrambling, making it fundamentally different in open quantum systems [32, 34,

59, 65, 67–73]. Also, generalizing familiar concepts from closed systems to open systems has led to the discovery of novel and intriguing physics including the development of entropy dynamics [74–77], operator growth and complexity [78–82], strong to weak symmetry breaking [83–88], quantum speed limit [89–94], generalize Lieb–Schultz–Mattis theorem in open systems [95, 96]. This raises a natural question: how do the dynamics of OTOC and LE behave in open quantum systems?

In this paper, we generalize the concepts of the LE and the OTOC to open quantum systems governed by the Lindblad master equation. Interaction with the environment enriches the dynamics of information scrambling, creating a complex interplay between quantum chaos and dissipation. We investigate the universal behavior of the LE, analyzing its dynamics in both weak and strong dissipation regimes. In the weak dissipation regime, we identify a universal structure for the LE and explain its characteristic behavior. In the strong dissipation regime, we discover that the LE can exhibit a two-local-minima structure, reflecting the Lindblad spectrum of the dissipative evolution. Additionally, we establish a connection between the thermal average of the LE and the OTOC and prove a general relation between the OTOC and Rényi entropy in open systems. Furthermore, we propose an experimental protocol for measuring the OTOC in open systems.

The structure of this paper is organized as follows. In Section II, we review the definition of the LE in closed systems, introduce its generalization to open systems, and discuss its physical significance. In Section III, we analyze the simplest case where the forward and backward evolutions of the LE in open systems differ only by the dissipation strength, exploring LE dynamics in both weak and strong dissipation regimes. In Section IV, we review the relation between the OTOC and the LE in closed systems, introduce the definition of the OTOC in

* zhouyn.physics@gmail.com

† changliu@nus.edu.sg

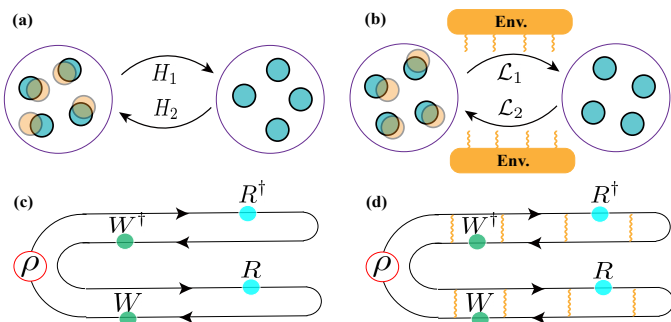


FIG. 1. Schematic of the LE in closed (a) and open systems (b), as well as the OTOC in closed (c) and open systems (d). (a): In closed systems, the forward and backward time evolutions are governed by different Hamiltonians (H_1 and H_2), resulting in a final state (orange circle) that differs from the initial state (blue circle). (b): In open systems, due to interactions with the environment (Env.), the Lindbladians \mathcal{L}_1 and \mathcal{L}_2 govern the forward and backward time evolutions, respectively. (c-d): The time contours of the OTOC. In contrast to the time evolution of OTOC in closed systems (c), the forward and backward time evolution in open systems have correlations, as denoted by the orange curved lines in (d).

open systems, and establish a similar OTOC-LE relation for open systems. In Section V, we extend the relation between the OTOC and Rényi entropy from closed systems to open systems. In Section VI, we propose an experimental protocol for measuring the OTOC in open quantum systems. Finally, in Section VII, we present our conclusions and discuss the implications of our findings.

II. THE LOSCHMIDT ECHO IN OPEN SYSTEMS

In an isolated quantum system, the LE measures the retrieval fidelity of a quantum state following an imperfect time-reversal evolution. It is defined as follows:

$$M(t) = |\langle \psi_0 | e^{iH_2 t} e^{-iH_1 t} | \psi_0 \rangle|^2. \quad (1)$$

Here, H_1 and H_2 are the Hamiltonian governing the forward and backward time evolution, respectively. $|\psi_0\rangle$ is the initial quantum state at time $t_0 = 0$. Consider the case where $H_2 = H_1 + V$, with V representing a perturbation to H_1 , thus, the LE measures the sensitivity of quantum evolution to the perturbation and quantifies the degree of irreversibility. Even small perturbations to the Hamiltonian can induce significant changes in the system's dynamics, resulting in a substantial deviation of the LE from 1 as the total evolution time increases from 0. The definition of the LE is illustrated schematically in Fig. 1(a).

In real experiments, the measurement of the LE has been performed in numerous nuclear magnetic resonance (NMR) studies since the 1950s [43–53], where echo experiments have served as a standard tool.

We generalize the definition of the LE for open systems and will further discuss its dynamics [40, 42] in the next section. Specifically, we consider the LE in open quantum systems coupled to a Markovian environment, where the dynamics are governed by the Lindblad master equation.

$$\frac{\partial \rho}{\partial t} = -i[H, \rho] + 2\gamma \sum_m L_m \rho L_m^\dagger - \gamma \sum_m \{L_m^\dagger L_m, \rho\}. \quad (2)$$

Here, the first term on the right-hand side (R.H.S.) describes the unitary time evolution with Hamiltonian H , while the remaining terms describe the interaction between the system and the environment, characterized by the Lindblad jump operators L_m and the dissipation strength γ . Below, we use $\rho(t) = e^{\mathcal{L}t}[\rho_0]$ to denote the density matrix obtained by evolving the initial density matrix ρ_0 under the Lindblad master equation for a total time t .

Considering a general density matrix ρ , and given a set of complete bases $\{|n\rangle\}$, the density matrix ρ can be expressed as

$$\rho = \sum_{m,n} \rho_{mn} |m\rangle\langle n|. \quad (3)$$

By using the Choi-Jamiołkowski isomorphism [97–99], the density matrix ρ can be mapped to a wave function $|\psi_\rho^D\rangle$ in double space, where

$$|\psi_\rho^D\rangle = \sum_{mn} \rho_{mn} |m\rangle_L \otimes |n\rangle_R. \quad (4)$$

Here, we denote the two copies of the system in double space as the left (L) and right (R) systems.

After this mapping, the Lindblad master equation, which describes the dynamics of the density matrix, can be transformed into a non-unitary Schrödinger-like equation that governs the dynamics of the double-space wave function $|\psi_\rho^D\rangle$ [74, 97–99]:

$$i\partial_t |\psi_\rho^D(t)\rangle = H^D |\psi_\rho^D(t)\rangle. \quad (5)$$

Here, $H^D = H_s - iH_d$ is a non-Hermitian operator defined on the double space with

$$\begin{aligned} H_s &= H_L \otimes \mathcal{I}_R - \mathcal{I}_L \otimes H_R^T, \\ H_d &= \gamma \sum_m [-2L_{m,L} \otimes L_{m,R}^* \\ &\quad + (L_m^\dagger L_m)_L \otimes \mathcal{I}_R + \mathcal{I}_L \otimes (L_m^\dagger L_m)_R^*], \end{aligned} \quad (6)$$

where the superscript “T” stands for the transpose, and * stands for the complex conjugation. Here, H_s is the Hermitian part of the double space Hamiltonian, determined by the system Hamiltonian. H_d originates from the dissipative part of the Lindblad evolution and is determined by the dissipation operators; hence, we refer to it as the “dissipative part of the double space Hamiltonian.”

Using this double-space representation, we can define the generalized LE in open systems as:

$$M^D(t) \equiv \frac{\text{Tr}[\rho_1(t)\rho_2(t)]}{\sqrt{\text{Tr}[\rho_1^2(t)]\text{Tr}[\rho_2^2(t)]}} = \frac{\langle \psi_0^D | e^{iH_2^D t} e^{-iH_1^D t} | \psi_0^D \rangle}{\sqrt{\langle \psi_0^D | e^{iH_1^D t} e^{-iH_1^D t} | \psi_0^D \rangle \langle \psi_0^D | e^{iH_2^D t} e^{-iH_2^D t} | \psi_0^D \rangle}}. \quad (7)$$

Here, $\rho_1(t) = e^{\mathcal{L}_1 t}[\rho_0]$ and $\rho_2(t) = e^{\mathcal{L}_2 t}[\rho_0]$. ρ_1 and ρ_2 represent the density matrix under the forward Lindblad superoperator \mathcal{L}_1 and backward Lindblad superoperator \mathcal{L}_2 respectively. $|\psi_0^D\rangle$ is the double space wave function obtained from the initial density matrix ρ_0 . H_1^D and H_2^D are the double-space Hamiltonians corresponding to the Lindblad superoperator \mathcal{L}_1 and \mathcal{L}_2 , respectively, as defined in Eq. (6). Thus, H_1^D and H_2^D can also be viewed as the forward and backward double-space Hamiltonians. The illustration of the generalized LE in the open system is depicted in Fig. 1(b).

Our definition of the generalized LE describes the system's departure from its initial state after undergoing forward lindblad evolution \mathcal{L}_1 followed by a distinct backward lindblad evolution \mathcal{L}_2 . Since the purity of the density matrix, $\text{Tr}[\rho^2(t)]$, generally decays due to the decoherence in open systems, even when the forward and backward time evolutions are identical ($\rho_1 = \rho_2$), the overlap $\text{Tr}[\rho_1(t)\rho_2(t)]$ can still decrease over time. To characterize the intrinsic differences between the forward and backward time evolution in open systems, we introduce the normalization factor $\sqrt{\text{Tr}[\rho_1^2(t)]\text{Tr}[\rho_2^2(t)]}$ in Eq. (7) to excluding the purity decay of the density matrix during Lindblad time evolution.

If the dissipation strengths γ_1 and γ_2 in the Lindblad superoperators \mathcal{L}_1 and \mathcal{L}_2 are set to zero, and the initial double-space wave function $|\psi^D\rangle = |\psi_0\rangle \otimes |\psi_0\rangle$ is purified from a pure state density matrix $\rho_0 = |\psi_0\rangle\langle\psi_0|$, then the generalized LE defined in Eq. (7) can be rewritten as

$$M^D(t)|_{\gamma_1=\gamma_2=0} = \text{Tr}(e^{-iH_1 t} \rho_0 e^{iH_1 t} e^{-iH_2 t} \rho_0 e^{iH_2 t}) = |\langle \psi_0 | e^{iH_2 t} e^{-iH_1 t} | \psi_0 \rangle|^2. \quad (8)$$

Hence, in the absence of dissipation, the generalized LE in an open system reduces to its definition in closed systems, as given by Eq. (1). In this context, it quantifies the quantum fidelity between two states after undergoing different Hamiltonian evolutions.

Additionally, the generalized LE can be interpreted as describing the overlap between two (mixed) density matrices. This overlap quantifies the similarity between the two mixed states and is related to the relative purity, which is defined as

$$F_{RP}(\rho_1, \rho_2) = \frac{\text{Tr}(\rho_1 \rho_2)}{\text{Tr}(\rho_1^2)}. \quad (9)$$

The rate of change of relative purity can signal quantum fluctuations and is often discussed in the context

of quantum speed limits [100–104]. It is worth noting that the only distinction between relative purity and the generalized LE we have defined lies in their respective normalization factors. Therefore, the generalized LE in open systems can also be used to analyze quantum speed limits.

III. THE LOSCHMIDT ECHO DYNAMICS IN OPEN SYSTEMS

In open systems, our generalized LE can be used to characterize the irreversibility between different forward and backward dissipative dynamics. In principle, the forward and backward Lindblad evolutions can differ in several aspects: the system Hamiltonian H , the dissipation strength γ , or the set of Lindblad jump operators $\{L_m\}$. In this work, to elucidate the role of dissipation, we consider the simplest case where the forward and backward evolutions share the same Hamiltonians and dissipation operators, differing only in the dissipation strengths γ .

We investigate the universal dynamical properties of the generalized LE and identify the characteristic time scales that arise from the interplay between the two different dissipation strengths of the Lindblad superoperator and the energy scales of the Hamiltonian.

Without loss of generality, we numerically study a dissipative Sachdev-Ye-Kitaev (SYK) model as an example to illustrate the typical dynamical behavior of the generalized LE in open systems. We consider a quantum system composed of N Majorana fermions, described by the SYK model Hamiltonian [105–108],

$$H_{\text{SYK}} = \sum_{1 \leq i < j < k < l \leq N} J_{ijkl} \chi_i \chi_j \chi_k \chi_l, \quad (10)$$

where χ_i denotes Majorana fermion operator satisfying the anticommutation relation $\{\chi_i, \chi_j\} = \delta_{ij}$. Here, J_{ijkl} is a random variable that satisfies the Gaussian distribution with zero mean and variance

$$\langle J_{ijkl} J_{i'j'k'l'} \rangle = \delta_{i,i'} \delta_{j,j'} \delta_{k,k'} \delta_{l,l'} \frac{3! J^2 (q-1)!}{N^3}.$$

We consider the set of jump operators $\{L_j = \chi_j\}$, ($j = 1, 2, \dots, N$) with dissipation strength γ [109], leading to the Lindblad time evolution:

$$\frac{\partial \rho}{\partial t} = -i[H_{\text{SYK}}, \rho] + 2\gamma \sum_{j=1}^N \chi_j \rho \chi_j - \gamma \sum_{j=1}^N \{\chi_j \chi_j, \rho\}. \quad (11)$$

Below, we use the dissipative SYK model as an example to study the dynamics of the LE in both the weak dissipation regime, where $\gamma/J \ll 1$, and the strong dissipation regime, where $\gamma/J \gg 1$. Our findings are summarized in Table III B. Without loss of generality, we denote the dissipation strengths of the forward and backward Lindblad evolutions as γ_1 and γ_2 , with $\gamma_1 < \gamma_2$. For clarity, we will refer to the Lindblad evolution with dissipation strengths γ_1 and γ_2 as the γ_1 evolution and γ_2 evolution, respectively.

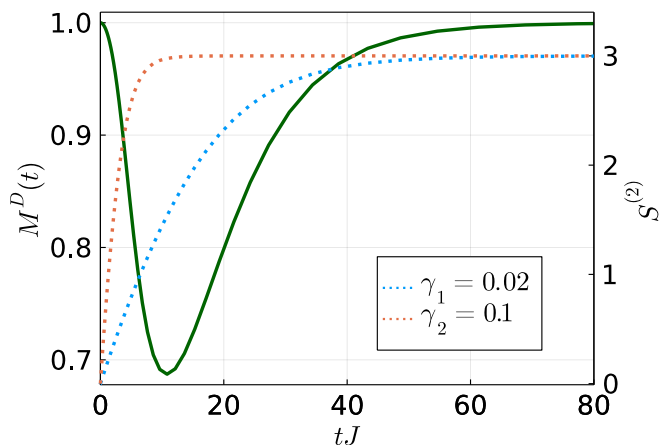


FIG. 2. The Loschmidt echo dynamics of the dissipative SYK model in the weak dissipation regime. We choose $N = 6$, $\gamma_1/J = 0.02$, and $\gamma_2/J = 0.1$, with dissipation applied to all Majorana fermions in the SYK model. The second Rényi entropy for the γ_1 and γ_2 evolutions are also plotted as blue and red dotted lines, respectively, for comparison. The initial state is the ground state of the SYK model. The time at which the Loschmidt echo reaches its minimum approximately coincides with the time when the second Rényi entropy for the smaller dissipation strength, γ_1 , saturates to its final plateau value.

A. Weak dissipation regime

In the weak dissipation regime, where $\gamma_{1,2}/J \ll 1$, the generalized LE exhibits a universal behavior, as illustrated in Fig. 2. The LE decays from its initial value of 1, reaching a minimum at the characteristic time scale t_{\min} . Subsequently, the LE increases and eventually returns to a plateau with a value of 1 at the time scale t_p .

For simplicity, we consider the case where the system has only one steady state, which is $\rho(t \rightarrow \infty) \propto \mathcal{I}$. Therefore, in the long-time limit, different dissipation strengths have no effect on the final states: both $\rho_1(t)$ and $\rho_2(t)$ approach the same steady state, and the LE returns to its initial value of 1.

The characteristic time scales t_{\min} and t_p in the weak dissipation regime are determined by the dissipation strengths. To understand these time scales, we can analyze the dynamics of the second Rényi entropy, which is defined as follows:

$$S^{(2)} = -\log [\text{Tr}(\rho^2)]. \quad (12)$$

The dynamics of the second Rényi entropy for ρ_1 and ρ_2 are shown in Fig. 2 by the blue and red dotted lines, respectively. For comparison, the green line represents the dynamics of the LE.

In the weak dissipation regime, the dynamics of the second Rényi entropy initially increase, following a characteristic γt scaling at short times [110], and eventually saturate as the initial state evolves toward the steady

state. Since $\gamma_1 < \gamma_2$, the time for $\rho_2(t)$ to reach its steady state is shorter than that of $\rho_1(t)$. The time t_{\min} represents the time when one quantum state (under γ_2 evolution) reaches its steady state and its entropy stops increasing, while the other state (under γ_1 evolution) has not yet reached its steady state. Therefore, at $t_{\min} \sim 1/\gamma_2$, the LE shows a minimum, as shown in Fig. 2.

The final plateau time $t_p \sim 1/\gamma_1$ is the time when both $\rho_1(t)$ and $\rho_2(t)$ reach the same steady state, at which point both of their entropies reach their maximum values, as depicted in Fig. 2, where the blue and red dotted lines saturate to the final plateau value.

B. Strong dissipation regime

The behavior of the LE becomes more complex when we consider the strong dissipation regime, where $\gamma_{1,2}/J \gg 1$. To analyze this, we use the double-space representation, where the time evolution of the density matrix is governed by the non-Hermitian double-space Hamiltonian $H^D = H_s - iH_d$, as defined in Eq. (6).

In the strong dissipation regime, H^D is dominated by its dissipation part, $-iH_d$, while its Hermitian part, H_s , can be treated as a perturbation. Under these conditions, the dynamics of the generalized LE vary significantly depending on whether the ground state of H_d is degenerate.

When the ground state of H_d is non-degenerate, the LE dynamics follow patterns similar to those seen in the weak dissipation regime. However, if H_d has degenerate ground states, we observe distinct behavior in the LE dynamics, including a potential two-local-minima structure, which can be attributed to the spectral structure of H^D in this case.

1. Ground state of H_d is non-degenerate

First, we consider the case where the dissipative Hamiltonian H_d has a non-degenerate ground state. For example, we examine the dissipative SYK model in Eq. (11), where dissipation acts on all Majorana fermions, i.e., $L_j = \chi_j$ for $j = 1, \dots, N$. In this model, the unique ground state of the dissipative Hamiltonian H_d is the EPR state in double space, which corresponds to the identity density matrix in the original Hilbert space.

In our numerical simulation, we choose the initial state as the ground state of the SYK Hamiltonian. In this scenario, the LE dynamics, as shown in Fig. 3(a), exhibit a structure similar to that observed in the weak dissipation regime. This is because the typical behavior is still primarily determined by dissipation dynamics, as in the weak dissipation regime: at time $t_{\min} \sim 1/\gamma_2$, ρ_2 with dissipation strength γ_2 nearly reaches its steady state, while the evolution under γ_1 still has non-vanishing dissipative components, causing the LE to reach a minimum. Then, at time $t_p \sim 1/\gamma_1$, both density matrices, ρ_1 and

Cases	Typical dynamical structure	Late time plateau
weak: $\gamma_1/J < \gamma_2/J \ll 1$	One minimum, $t_{\min} \sim 1/\gamma_2$	$t_p \sim 1/\gamma_1$
strong (non-degenerate): $1 \ll \gamma_1/J < \gamma_2/J$	One minimum, $t_{\min} \sim 1/\gamma_2$	$t_p \sim 1/\gamma_1$
strong (degenerate): $1 \ll \gamma_1/J < \gamma_2/J$	Two local minima, $t_{\min 1} \sim 1/\gamma_2$, $t_{\min 2} \sim \gamma_1/J^2$	$t_p \sim \gamma_2/J^2$

TABLE I. Summary of the generalized Loschmidt echo dynamics in the weak and strong dissipation regimes. For the strong dissipation regime, the dynamics are further classified based on whether the ground state of H_d is degenerate or non-degenerate.

ρ_2 , reach their steady states, and the LE saturates to a plateau.

2. Ground state of H_d is degenerate

Next, we consider the case where the dissipative Hamiltonian H_d has degenerate ground states. As an example, we examine a deformation of the dissipative SYK model, where only half of the Majorana fermions (with indices $j = 1, 2, \dots, \frac{N}{2}$) in the system are coupled to the environment. Under these conditions, the system's density matrix evolves as follows:

$$\frac{\partial \rho}{\partial t} = -i[H_{\text{SYK}}, \rho] + 2\gamma \sum_{j=1}^{N/2} \chi_j \rho \chi_j - \gamma \sum_{j=1}^{N/2} \{\chi_j \chi_j, \rho\}. \quad (13)$$

The ground state degeneracy of H_d arises because dissipation only affects the degrees of freedom in one half of the system (Majorana fermions χ_j for $j = 1, 2, \dots, \frac{N}{2}$), leaving the energy of H_d invariant in the other half. As a result, any pairing operator involving an even number of these undissipated Majorana fermions, such as $\chi_{j_1} \chi_{j_2}$ (with $j_1, j_2 = \frac{N}{2} + 1, \dots, N$), corresponds to a ground state of H_d .

In our numerical simulation, we choose the initial state as the ground state of the SYK Hamiltonian. This initial state contains components outside the ground-state Hilbert space of H_d , as the SYK Hamiltonian does not commute with H_d . Consequently, we observe that the generalized LE exhibits distinct dynamical behavior, characterized by a two-local-minima structure, as shown in Fig. 3(b).

This novel structure is determined by the spectrum of H_D , which corresponds to the spectrum of the Lindblad superoperator and is referred to as the Lindblad spectrum. In the strong dissipation regime, the Lindblad spectrum exhibits two distinct energy scales, as illustrated in Fig. 4. This separation of energy scales leads to contrasting behaviors in the short-time and long-time dynamics: as the dissipation strength increases, the short-time dynamics accelerate, while the long-time dynamics slow down.

More explicitly, the main feature of the Lindblad spectrum in the strong dissipation regime is that it separates into segments along the imaginary axis. Since H^D is dominated by its dissipation part $-iH_d$ with dissipation strength γ , the separations between these segments are on the order of γ . Within each segment, the perturbative term H_s in the double space Hamiltonian H^D with

energy scale J determines the finer structure, resulting in widths along the imaginary axis on the order of J^2/γ , as depicted in Fig. 4. We refer to the eigenstates with imaginary parts on the order of a few times γ as high imaginary energy states, and the eigenstates with imaginary parts on the order of J^2/γ as low-lying imaginary energy states [74].

For a general Lindblad evolution with this segmented Lindblad spectrum structure, the short-time dynamics are dominated by high-imaginary-energy states, which have imaginary components on the order of γ , leading to dynamics on the γt scale. In the long-time limit, these high-imaginary-energy states decay, and the dynamics become dominated by low-lying imaginary-energy states, with imaginary components on the order of J^2/γ . As a result, the long-time dynamics follow the $J^2 t/\gamma$ scale.

With the above analysis of the Lindblad spectrum, we can now discuss the LE dynamics in the strong dissipation regime. Recall that we consider the case where the dissipation for both forward and backward evolutions (γ_1 and γ_2 evolution) has the same form, differing only in dissipation strength. As a result, the eigenstates of the double-space Hamiltonian for the forward and backward evolutions are nearly identical. Consequently, as we will demonstrate, the generalized LE exhibits a local maximum at intermediate times and a long-time plateau at a value of 1, due to the near alignment of eigenstates in the γ_1 and γ_2 evolutions.

The times at which the first and second local minima of the generalized LE occur are denoted as $t_{\min 1}$ and $t_{\min 2}$ respectively, with the local maximum between them marked as t_{\max} . The time at which the LE reaches its final plateau is denoted as t_p . Below, we analyze the events occurring at each of these time points in chronological order and provide a brief discussion of the timescales associated with them.

- First local minimum: $t_{\min 1}$.

The initial decrease of the generalized LE is due to the differing decay rates of high imaginary energy states in the γ_1 and γ_2 evolutions. The time $t_{\min 1}$ corresponds to the point when high imaginary energy states have mostly decayed in the γ_2 evolution but remain significant in the γ_1 evolution. Since the short-time dynamics follow the γt timescale, we have $t_{\min 1} \simeq \frac{1}{\gamma_2}$. After $t_{\min 1}$, the γ_2 evolution predominantly occupies low-lying imaginary energy states, while the high imaginary energy states in the γ_1 evolution, which are nearly orthogonal to the states in γ_2 , begin to decay gradually. Conse-

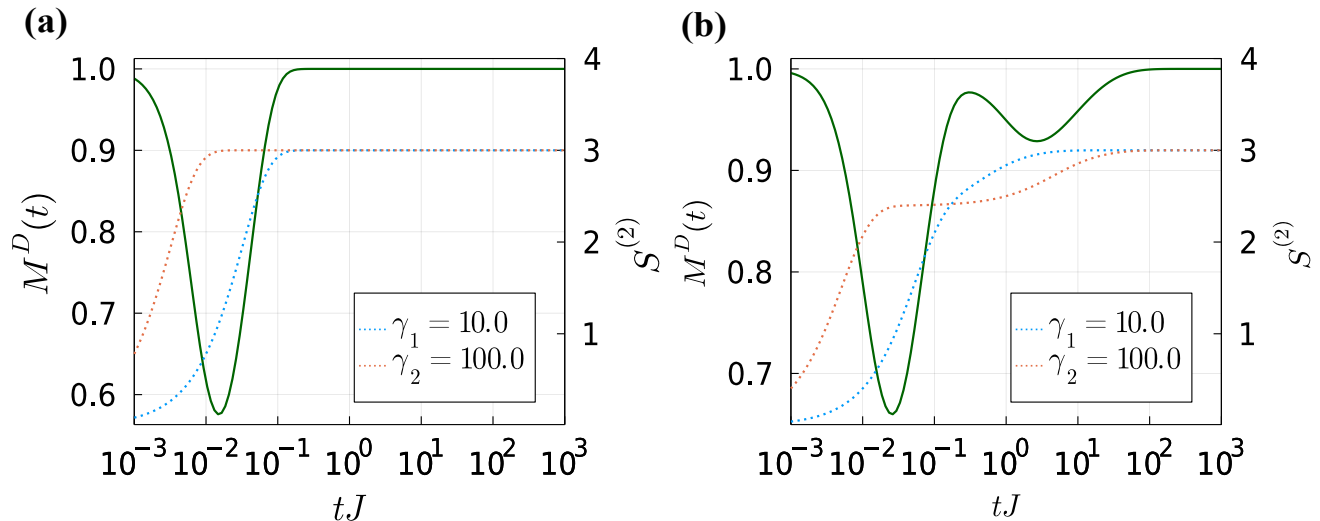


FIG. 3. The Loschmidt echo dynamics of the dissipative SYK model in the strong dissipation regime. Here, we choose $N = 6$, $\gamma_1/J = 10$, and $\gamma_2/J = 100$, with the initial state being the ground state of the SYK model. In panel (a), dissipation is applied to all Majorana fermions, resulting in a non-degenerate ground state of H_d , while in panel (b), dissipation is applied to half of the Majorana fermions, leading to a degenerate ground state of H_d . The second Rényi entropy for γ_1 and γ_2 evolution are also plotted as the blue and red dot lines for comparison. The LE in (a) exhibits a single minimum structure, while the LE in (b) shows a two-local-minima structure.

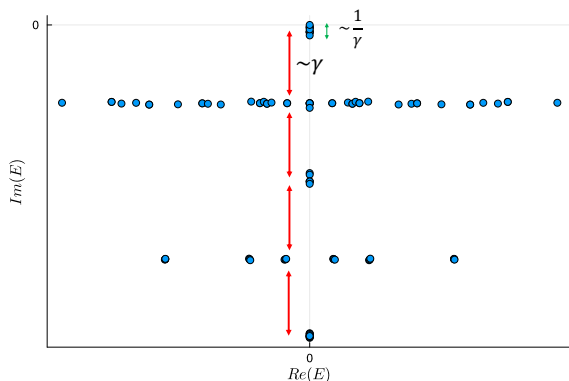


FIG. 4. The schematic diagram illustrates the spectrum of H_D in the strong dissipation regime, where the spectrum splits into segments along the imaginary axis, spaced by intervals on the order of γ . The ground state degeneracy of H_D is indicated by the presence or absence of a border around the segment near zero, with this border having a width on the order of J^2/γ . The figure shows the case where the ground states of H_D are degenerate, highlighted by the bordered segment near zero. In contrast, if the ground state is non-degenerate, the segment around zero appears without this border.

quently, the difference between the density matrices ρ_1 and ρ_2 decreases, leading to an increase in the LE after $t_{\min 1}$.

- **Local maximum: t_{\max} .**
The local maximum occurs when the high-imaginary-energy states of the γ_1 evolution decay.

At this point, both evolutions are predominantly distributed over low-lying imaginary energy states, resulting in the overlap between the density matrices ρ_1 and ρ_2 reaching a local maximum. Subsequently, the low-lying imaginary energy states begin to decay around $t \sim \frac{J^2}{\gamma}$ for the γ_1 evolution. As a result, the LE decreases again, since the decay rates of the low-lying imaginary energy states for γ_1 and γ_2 evolutions are different.

- **Second local minimum: $t_{\min 2}$.**
At $t_{\min 2}$, the low-lying imaginary energy states have decayed for the γ_1 evolution, while they persist for the γ_2 evolution. At this time point, the γ_1 evolution approaches its steady state, whereas the γ_2 evolution has not yet reached a steady state. Given that the long-time dynamics scale as $\frac{J^2}{\gamma}t$ scale, the $t_{\min 2} \sim \frac{\gamma_1}{J^2}$.
- **Long-time plateau: t_p .**
Following $t_{\min 2}$, the low-lying imaginary energy states for the γ_2 evolution gradually decay, reaching steady state at $t_p \sim \frac{J^2}{\gamma^2}$. At this point, the LE reaches its final plateau value of 1, indicating that both evolutions have reached their respective steady states.

We compare the dynamics of the generalized LE with that of the second Rényi entropy for γ_1 and γ_2 evolutions in Fig. 3(b). The second Rényi entropy dynamics for ρ_1 and ρ_2 are shown by the blue and red dotted lines, respectively, while the LE dynamics are represented by

the green line for comparison. As illustrated in Fig. 3(b), the timescale of the LE's first minimum, $t_{\min 1}$, coincides with the point when the Rényi entropy dynamics of the γ_2 evolution reach their first plateau (means that the high imaginary energy states for γ_2 evolution decay out, while its low-lying imaginary energy states have not decayed yet). In contrast, the γ_1 evolution has not yet reached its first plateau, indicating that the high imaginary energy states are still present.

Similarly, the timescale of the LE's second minimum, $t_{\min 2}$, aligns with the maximum value of the Rényi entropy for the γ_1 evolution. This indicates that the low-lying imaginary energy states in γ_1 evolution have decayed, allowing it to reach a steady state, while the γ_2 evolution has not yet reached its maximum entropy. Finally, the time at which the LE reaches its final plateau coincides with the point at which the Rényi entropy dynamics of the γ_2 evolution reach their final saturation. After this point, both evolutions reach their steady states.

IV. THE OTOC-LOSCHMIDT ECHO RELATION IN OPEN SYSTEMS

The out-of-time-ordered correlator (OTOC) is a widely used diagnostic tool for detecting quantum chaos, as it measures quantum information scrambling and the system's sensitivity to initial conditions. In a closed system, it is defined as a four-point correlator with an unconventional time-ordering

$$F_\beta(t) \equiv \langle R_B^\dagger(t) W_A^\dagger R_B(t) W_A \rangle_\beta. \quad (14)$$

Here, $R_B(t) = e^{iHt} R_B e^{-iHt}$ represents the time evolution of the operator R_B , $\langle \cdot \rangle_\beta$ denotes thermal average at temperature $1/\beta$. Below, we consider the infinite temperature case for simplicity. Thus, $F(t) \equiv \text{Tr} [R_B^\dagger(t) W_A^\dagger R_B(t) W_A] / d$, where d is the dimension of the Hilbert space.

Both OTOC and LE describe the irreversibility induced by perturbations, and they are connected through the OTOC-LE relation in closed systems [56]. In real systems, dissipation is inevitable, which raises the question: does this relation also hold in dissipative settings? In this section, we extend the definition of OTOC and establish a generalized OTOC-LE relation for open systems.

A. OTOC-LE relation in closed systems

We first review how OTOC and LE are related in closed systems. Following the approach in [56], consider a bipartite system where A is a small subsystem and B is its complement. We choose W_A and R_B in Eq. (14) to be local unitary operators defined in subsystem A and B , respectively. Since the dynamical behavior of the OTOC

is universal for a chaotic Hamiltonian, which is insensitive to the specific choices of the operators W_A and R_B , as long as they do not reflect the particular symmetries of the Hamiltonian, we can consider the average OTOC over all unitary operators support on subsystems A and B ,

$$\overline{F(t)} = \frac{1}{d} \int dW_A dR_B \text{Tr} [R_B^\dagger(t) W_A^\dagger R_B(t) W_A]. \quad (15)$$

Here, the integration is performed with respect to the Haar measure for unitary operators.

With the aid of the formula for the Haar integral

$$\int dW_A W_A^\dagger O W_A = \frac{1}{d_A} \mathcal{I}_A \otimes \text{Tr}_A(O), \quad (16)$$

the average OTOC in Eq. (15) can be written as

$$\begin{aligned} \overline{F(t)} &= \frac{1}{d_A d} \int dR_B \text{Tr} \left\{ \mathcal{I}_A \otimes \text{Tr}_A [R_B(t)] R_B^\dagger(t) \right\} \\ &= \frac{1}{d_A d} \int dR_B \text{Tr}_B \left\{ \text{Tr}_A [R_B(t)] \text{Tr}_A [R_B^\dagger(t)] \right\}. \end{aligned} \quad (17)$$

Thus, the OTOC is related to the reduced evolution of the operator $\text{Tr}_A [R_B(t)] = \text{Tr}_A (e^{iHt} R_B e^{-iHt})$.

Without loss of generality, the total system Hamiltonian can be written as

$$H = H_A + H_B + V. \quad (18)$$

Here, H_A and H_B are the Hamiltonians defined on subsystems A and B , respectively. The interaction term is given by $V = \delta \sum_k V_A^k \otimes V_B^k$, where δ represents the coupling constant between subsystems A and B . To account for the effect of the coupling on the reduced evolution of the operator R_B , we approximately treat it as random noises acting on subsystem B [56, 111, 112],

$$\text{Tr}_A (e^{iHt} R_B e^{-iHt}) \simeq d_A \overline{e^{i(H_B + V_\alpha)t} R_B e^{-i(H_B + V_\alpha)t}}. \quad (19)$$

Here, $\{V_\alpha\}$ denotes the random noise operator, and the overline represents the average over all the realizations of $\{V_\alpha\}$ [113].

Using the above approximation and the Haar integral in Eq. (16) to compute the random average over R_B , the average OTOC in Eq. (15) can be further written as

$$\overline{F(t)} \simeq \frac{1}{d_B^2} \overline{|\text{Tr}_B [e^{-i(H_B + V_\alpha)t} e^{i(H_B + V_{\alpha'})t}]|^2}, \quad (20)$$

where R.H.S represents the average over all realizations of the noise operators $\{V_\alpha\}$ and $\{V_{\alpha'}\}$. Each term in this average corresponds to the LE as defined in Eq. (1). Thus, we obtain the OTOC-LE relation in closed systems. We also provide proof of this OTOC-LE relation using the diagram representation in Appendix A [114].

B. Generalization of OTOC-LE relation to open systems

We proceed by defining the OTOC in open systems and demonstrate that a generalized OTOC-LE relation also holds in open systems. Previous studies have proposed various definitions for the OTOC in open systems [53, 58–66]. Here, we adopt the definition that is particularly suitable for future experimental realizations, such as those using NMR techniques. The experimental implementation using NMR will be discussed in detail in Section VI.

The definition of the OTOC in open systems is extended as follows:

$$F^D(t) = \frac{1}{d} \text{Tr} \left\{ R_B^\dagger e^{\mathcal{L}^\dagger t} \left[W_A^\dagger e^{\mathcal{L}t} [R_B] W_A \right] \right\}. \quad (21)$$

Here $e^{\mathcal{L}t}[R]$ represents the dynamical evolution of an operator R under the operator Lindblad equation:

$$\frac{\partial R}{\partial t} = i[H, R] + 2\gamma \sum_m L_m^\dagger R L_m - \gamma \sum_m \{L_m^\dagger L_m, R\} \quad (22)$$

for a total time t . Note that a minus sign should precede the $\sum_m L_m^\dagger R L_m$ term when both R and L_m are fermionic operators [80, 115].

The term $e^{\mathcal{L}^\dagger t}[R]$ represents the backward evolution of an operator R under the operator Lindblad equation:

$$\frac{\partial R}{\partial t} = -i[H, R] + 2\gamma \sum_m L_m^\dagger R L_m - \gamma \sum_m \{L_m^\dagger L_m, R\}. \quad (23)$$

We also define $e^{\tilde{\mathcal{L}}t}[R]$ through the relation

$$\text{Tr} [R e^{\mathcal{L}t}[W]] = \text{Tr} [e^{\tilde{\mathcal{L}}t}[R]W],$$

which represents the adjoint dynamical evolution of an operator R under the equation:

$$\frac{\partial R}{\partial t} = -i[H, R] + 2\gamma \sum_m L_m R L_m^\dagger - \gamma \sum_m \{L_m^\dagger L_m, R\}. \quad (24)$$

When the system and bath are decoupled, meaning the dissipation strength in the Lindblad evolution is set to zero, the OTOC definition reduces to that of closed systems, as given in Eq. (14). Additionally, if all jump operators are Hermitian, we have $e^{\tilde{\mathcal{L}}^\dagger t}[R] = e^{\mathcal{L}t}[R]$.

Similarly, we consider the average OTOC in open systems by averaging over unitary operators on subsystems A and B :

$$\overline{F^D(t)} = \frac{1}{d} \int dW_A dR_B \text{Tr} \{ R_B^\dagger e^{\mathcal{L}^\dagger t} [W_A^\dagger e^{\mathcal{L}t} [R_B] W_A] \}. \quad (25)$$

We denote the OTOC of the open system as F^D , distinguishing it from the OTOC of closed systems. Here, W_A and R_B represent random unitary operators acting on

subsystems A and B , respectively. Averaging the OTOC over the random unitary operators W_A yields

$$\begin{aligned} & \int dW_A F^D(t) \\ &= \frac{1}{d_A} \text{Tr} \left\{ \mathcal{I}_A \otimes \text{Tr}_A [e^{\mathcal{L}t} [R_B]] e^{\tilde{\mathcal{L}}^\dagger t} [R_B^\dagger] \right\} \\ &= \frac{1}{d_A} \text{Tr}_B \left\{ \text{Tr}_A [e^{\mathcal{L}t} [R_B]] \text{Tr}_A [e^{\tilde{\mathcal{L}}^\dagger t} [R_B^\dagger]] \right\}. \end{aligned} \quad (26)$$

We then apply an approximation similar to that used in closed systems [116], where the effect of the coupling on the reduced evolution of the operator R_B is approximated as random noise, represented by V_α , acting on subsystem B . This approximation leads to the expression:

$$\text{Tr}_A [e^{\mathcal{L}t} [R_B]] \simeq d_A \overline{e^{\mathcal{L}_{B,\alpha}t} [R_B]},$$

the average OTOC further becomes

$$\overline{F(t)} \simeq \frac{1}{d_B} \int dR_B \overline{\text{Tr}_B \{ e^{\mathcal{L}_{B,\alpha}t} [R_B] e^{\tilde{\mathcal{L}}_{B,\alpha'}^\dagger t} [R_B^\dagger] \}} \quad (27)$$

Here, α labels different realizations of the noise. $e^{\mathcal{L}_{B,\alpha}t}[R_B]$ represents the effective Lindblad evolution of operator R_B under the Lindblad evolution

$$\frac{\partial R}{\partial t} = -i[H + V_\alpha, R] + 2\gamma \sum_m L_m^\dagger R L_m - \gamma \sum_m \{L_m^\dagger L_m, R\}. \quad (28)$$

For simplicity, we have omitted the subscript B in the above equation. The overline in (27) denotes the average over the random realizations of the noise operators $\{V_\alpha\}$ and $\{V_{\alpha'}\}$ acting on subsystem B .

For a general bipartite open system governed by the Lindblad evolution, we apply the Choi-Jamiolkowski isomorphism to map the evolution into a doubled Hilbert space. In this representation, the Hamiltonian in the doubled space can be formulated as:

$$H^D = H_A^D + H_B^D + V^D.$$

Here,

$$H_{A/B}^D = H_{s,A/B} + H_{d,A/B},$$

and

$$V^D = V_L \otimes \mathcal{I}_R - \mathcal{I}_L \otimes V_R^T,$$

where $H_{s,A/B}$ and $H_{d,A/B}$ are defined as in Eq. (6).

After mapping to the doubled space, the average OTOC can be expressed as

$$\begin{aligned} & \overline{F^D(t)} \\ &= \frac{1}{d_B} \int dR_B \overline{\text{Tr}_B \{ e^{-i(H_B^D + V_\alpha^D)t} |R_B\rangle \langle R_B| e^{i(H_B^{D\dagger} + V_{\alpha'}^{D\dagger})t} \}} \\ &= \frac{1}{d_B^2} \overline{\text{Tr}_B \left[e^{i(H_B^{D\dagger} + V_{\alpha'}^{D\dagger})t} e^{-i(H_B^D + V_\alpha^D)t} \right]}. \end{aligned} \quad (29)$$

We then compare the above results with Eq. (7) and find that the averaged OTOC corresponds to the thermal average of (unnormalized) LE in open systems. This establishes a generalized relation between two distinct measures of information scrambling—OTOC and LE—applicable to open quantum systems governed by Lindblad time evolution. The connection between the OTOC and LE offers valuable insights into their dynamics in open systems, particularly in understanding quantum chaos within dissipative environments. A diagrammatic proof of this OTOC-LE relation in open systems is given in Appendix B [114].

V. THE OTOC-RÉNYI ENTROPY RELATION IN OPEN SYSTEMS

In the following, we will demonstrate that the normalization factor for the LE in open systems, which is the purity of the density matrix, is also related to the average of the OTOC. We begin by reviewing the relation between the OTOC and Rényi entropy in the closed system (a diagrammatic proof of this OTOC-Rényi entropy relation can be found in [55]). We will then show that this relation holds in open systems as well.

We consider a system initialized at infinite temperature $\rho \propto \mathcal{I}$, then it is quenched by an arbitrary operator O at time $t = 0$. Thus, $\rho(0) = OO^\dagger$. The density matrix at time t is then given by $\rho(t) = U(t)OO^\dagger U^\dagger(t)$. $U(t) = e^{-iHt}$ is the time evolution operator. We divide the total system into subsystems A and B, the reduced density matrix of subsystem A is

$$\rho_A(t) = \text{Tr}_B [\rho(t)] = \text{Tr}_B [U(t)OO^\dagger U^\dagger(t)]. \quad (30)$$

We consider the second Rényi entropy $S_A^{(2)}$ for the subsystem A defined as

$$S_A^{(2)} = -\log [\text{Tr}_A(\rho_A^2)]. \quad (31)$$

We consider the case of infinite temperature for simplicity. The OTOC is then defined as

$$F(t) = \text{Tr} [V^\dagger(t)R_B^\dagger V(t)R],$$

where we choose $V \equiv \rho(0) = OO^\dagger$. A general relation connecting the OTOC and the second Rényi entropy can be obtained by considering the average OTOC over the operator R_B [55]

$$\begin{aligned} & \int dR_B \text{Tr} [V^\dagger(t)R_B^\dagger V(t)R_B] \\ &= \frac{1}{d_B} \text{Tr} [\text{Tr}_B[V(t)] \otimes \mathcal{I}_B V(t)] \\ &= \text{Tr}_A [\text{Tr}_B[V(t)] \text{Tr}_B[V(t)]] \\ &= \text{Tr}_A(\rho_A^2). \end{aligned} \quad (32)$$

Here, R_B is a local unitary operator defined in subsystem B. The integral is performed over unitary operators

with respect to the Haar measure. However, it is worth noting that the random operator R_B only needs to satisfy the requirements of a unitary 1-design and does not necessarily need to be Haar random. In the second line of the equation above, we have applied the formula

$$\int dR_B R_B^\dagger V R_B = \frac{1}{d_B} \text{Tr}_B(V) \otimes I_B, \quad (33)$$

and $V = V^\dagger = \rho(0)$. Thus, we obtain a general relation between the OTOC and the second Rényi entropy,

$$\exp(-S_A^{(2)}) = \int dR_B \text{Tr} [V^\dagger(t)R_B^\dagger V(t)R_B]. \quad (34)$$

Below, we show that this relation still holds in open systems:

$$\exp(-S_A^{(2)}) = \int dR_B \text{Tr} \left\{ V^\dagger e^{\mathcal{L}^\dagger t} \left[R_B^\dagger e^{\mathcal{L}t} [V] R_B \right] \right\}, \quad (35)$$

where the Lindblad operators are assumed to be Hermitian, which implies $e^{\tilde{\mathcal{L}}^\dagger t} = e^{\mathcal{L}t}$. The reduced density matrix of subsystem A of the open system is given by:

$$\rho_A(t) = \text{Tr}_B \rho(t) = \text{Tr}_B [e^{\mathcal{L}t}[V]]. \quad (36)$$

Use the Eq. (33), the R.H.S of the Eq. (35) can be rewritten as

$$\begin{aligned} & \int dR_B \text{Tr} \left\{ V^\dagger e^{\mathcal{L}^\dagger t} \left[R_B^\dagger e^{\mathcal{L}t} [V] R_B \right] \right\} \\ &= \frac{1}{d_B} \text{Tr} \{ e^{\tilde{\mathcal{L}}^\dagger t} [V] (\text{Tr}_B e^{\mathcal{L}t} [V]) \otimes I_B \} \\ &= \text{Tr}_A \left[(\text{Tr}_B e^{\tilde{\mathcal{L}}^\dagger t} [V]) (\text{Tr}_B e^{\mathcal{L}t} [V]) \right] \\ &= \text{Tr}_A [\rho_A^2] \\ &= \exp(-S_A^{(2)}). \end{aligned} \quad (37)$$

The fourth line follows from $e^{\tilde{\mathcal{L}}^\dagger t} = e^{\mathcal{L}t}$. Additionally, we used $V^\dagger = V$ since $V = OO^\dagger$. This completes the proof of Eq. (35).

This relation, as given in Eq. (35), demonstrates that in open systems, the second Rényi entropy can be used to infer properties of the OTOC. The L.H.S. of the equation represents the Rényi entropy, which can be measured in a quench experiment, while the R.H.S. represents an equilibrium average with respect to the infinite-temperature density matrix. This establishes a connection between correlations evaluated in an equilibrium density matrix and quantities measured in non-equilibrium processes. Analogous to linear response theory—where a normal correlator measures the response of observables to a perturbation of the system's Hamiltonian, the OTOC measures the response of the system's entropy to a quench [55].

In this section and the previous one, we separately consider the non-normalized LE and the normalization factor of LE. The non-normalized LE is related to the average

OTOC, while the normalization factor, which is directly related to the Rényi entropy, is also linked to the average OTOC. This approach aligns with real experimental conditions, where these quantities are more naturally measured independently and then combined to define the LE in the open system.

VI. THE EXPERIMENT PROTOCOL OF MEASURING OTOC

In closed systems, the OTOC has been experimentally measured on various platforms, including NMR [28, 29], superconducting circuits [30–32], trapped ions [33–35], and cold atoms [36]. Below, we outline a straightforward protocol for measuring the OTOC defined in Eq. (21) in open systems, using an NMR experimental setup as an example.

This protocol involves the following steps:

- **1. Initial state preparation:** Prepare the system in a high-temperature state ρ_0 with a polarization field M_B [28]:

$$\rho_0 \propto e^{-\beta(H-hM_B)} \simeq \mathcal{I} - \epsilon M_B. \quad (38)$$

Here, \mathcal{I} represents the identity operator. Since \mathcal{I} remains constant and does not affect observables under Lindblad dynamics, we treat the density matrix as effectively proportional to M_B .

- **2. Forward Evolution:** Evolve the system with forward Lindblad evolution, then the system's density matrix becomes $e^{\mathcal{L}t}[M_B]$.
- **3. Apply Perturbation:** Apply an operator W_A to the system, resulting in the modified density matrix: $\rho_1 = W_A^\dagger e^{\mathcal{L}t}[M_B] W_A$.
- **4. Backward Evolution:** Evolve the system with backward Lindblad dynamics, yielding the final state $\rho_2 = e^{\mathcal{L}^\dagger t} [W_A^\dagger e^{\mathcal{L}t}[M_B] W_A]$.
- **5. Measurement:** Measure the operator M_B on the final state ρ_2 .

The expectation value M_B on the final state provides the OTOC:

$$\text{Tr}[\rho_2 M_B] = \text{Tr} \left\{ M_B e^{\mathcal{L}^\dagger t} \left[W_A^\dagger e^{\mathcal{L}t}[M_B] W_A \right] \right\}. \quad (39)$$

This expression matches the OTOC for an open system as defined in Eq. (21) if we set $R_B = M_B$, and assume $M_B = M_B^\dagger$. Consequently, this protocol can be employed to experimentally measure the OTOC in open systems.

VII. CONCLUSION AND SUMMARY

In this paper, we developed a framework to generalize the LE for open quantum systems and analyzed its dynamics using the Choi-Jamiolkowski isomorphism, which maps quantum evolution onto a doubled Hilbert space. We explored the relation between LE dynamics and the structure of the Lindblad spectrum. In the weak dissipation regime, the LE exhibits a one-minimum structure. In contrast, in the strong dissipation regime, the LE can display a two-local-minima structure, depending on whether the ground state of the dissipation part of the double-space Hamiltonian is degenerate. While this work primarily considers differences in dissipation strength between forward and backward Lindblad evolutions, future investigations could examine cases involving variations in dissipation forms or Hamiltonian components. Such studies could reveal additional universal structures in LE dynamics.

Additionally, we extended the definition of the OTOC to open systems. Our proposed definition is well-suited for probing universal information-scrambling properties in open quantum systems and can be experimentally measured using techniques like NMR. We demonstrated that the unnormalized LE in an open system is directly related to the average OTOC, paralleling the OTOC-LE relation in closed systems. Furthermore, we proved that the relation between the OTOC and the second Rényi entropy persists in open systems, establishing links between different measures of information scrambling. Future research could further generalize the connections among various information-scrambling measures in open systems, such as the spectral form factor, relative entropy, and operator entanglement [54, 57]. These efforts would deepen our understanding of information dynamics in dissipative quantum systems and open new directions for both experimental and theoretical investigations.

Lastly, it would be interesting to explore the symmetry aspects of LE dynamics [117]. For example, if the forward evolution respects certain symmetries while the backward evolution weakly breaks them, one could investigate how this weak symmetry breaking influences the LE dynamics. Our definition of the LE, which quantifies the similarity between two density matrices over time, could also be applied to study phase transitions during this process. In particular, it might serve as an order parameter for the transition from strong to weak symmetry breaking [83–88], which can only occur in mixed states. Moreover, it would be interesting to investigate the symmetry properties of two Lindblad evolutions [118–121] using our generalized LE shows promise for classifying the symmetry classes of different Lindbladians.

Acknowledgment. We would like to thank Hui Zhai for introducing us to this interesting topic and for his many insightful discussions. We also thank Tian-Gang Zhou for his valuable feedback and advice in revising the manuscript.

- [1] A. Larkin and Y. N. Ovchinnikov, Quasiclassical method in the theory of superconductivity, *Sov Phys JETP* **28**, 1200 (1969).
- [2] A. Kitaev, A simple model of quantum holography, Entanglement in strongly-correlated quantum matter, 38 (2015).
- [3] A. Almheiri, D. Marolf, J. Polchinski, D. Stanford, and J. Sully, An apologia for firewalls, *J. High Energ. Phys.* **2013** (9), 18.
- [4] S. H. Shenker and D. Stanford, Black holes and the butterfly effect, *J. High Energ. Phys.* **2014** (3), 67.
- [5] D. A. Roberts and D. Stanford, Diagnosing Chaos Using Four-Point Functions in Two-Dimensional Conformal Field Theory, *Phys. Rev. Lett.* **115**, 131603 (2015).
- [6] D. A. Roberts, D. Stanford, and L. Susskind, Localized shocks, *J. High Energ. Phys.* **2015** (3), 51.
- [7] S. H. Shenker and D. Stanford, Stringy effects in scrambling, *J. High Energ. Phys.* **2015** (5), 132.
- [8] P. Hosur, X.-L. Qi, D. A. Roberts, and B. Yoshida, Chaos in quantum channels, *J. High Energ. Phys.* **2016** (2), 4.
- [9] J. Maldacena, S. H. Shenker, and D. Stanford, A bound on chaos, *J. High Energ. Phys.* **2016** (8), 106.
- [10] D. Stanford, Many-body chaos at weak coupling, *J. High Energ. Phys.* **2016** (10), 9.
- [11] J. Maldacena, D. Stanford, and Z. Yang, Conformal symmetry and its breaking in two-dimensional nearly anti-de Sitter space, *Prog. Theor. Exp. Phys.* **2016**, 12C104 (2016).
- [12] J. Maldacena and D. Stanford, Remarks on the Sachdev-Ye-Kitaev model, *Phys. Rev. D* **94**, 106002 (2016).
- [13] G. Zhu, M. Hafezi, and T. Grover, Measurement of many-body chaos using a quantum clock, *Phys. Rev. A* **94**, 062329 (2016).
- [14] Y. Gu, X.-L. Qi, and D. Stanford, Local criticality, diffusion and chaos in generalized Sachdev-Ye-Kitaev models, *J. High Energ. Phys.* **2017** (5), 125.
- [15] M. Gärttner, J. G. Bohnet, A. Safavi-Naini, M. L. Wall, J. J. Bollinger, and A. M. Rey, Measuring out-of-time-order correlations and multiple quantum spectra in a trapped-ion quantum magnet, *Nature Phys* **13**, 781 (2017).
- [16] Y. Chen, H. Zhai, and P. Zhang, Tunable quantum chaos in the Sachdev-Ye-Kitaev model coupled to a thermal bath, *J. High Energ. Phys.* **2017** (7), 150.
- [17] X. Chen, R. Fan, Y. Chen, H. Zhai, and P. Zhang, Competition between Chaotic and Nonchaotic Phases in a Quadratically Coupled Sachdev-Ye-Kitaev Model, *Phys. Rev. Lett.* **119**, 207603 (2017).
- [18] X.-Y. Song, C.-M. Jian, and L. Balents, Strongly Correlated Metal Built from Sachdev-Ye-Kitaev Models, *Phys. Rev. Lett.* **119**, 216601 (2017).
- [19] A. A. Patel, D. Chowdhury, S. Sachdev, and B. Swingle, Quantum Butterfly Effect in Weakly Interacting Diffusive Metals, *Phys. Rev. X* **7**, 031047 (2017).
- [20] C. W. von Keyserlingk, T. Rakovszky, F. Pollmann, and S. L. Sondhi, Operator Hydrodynamics, OTOCs, and Entanglement Growth in Systems without Conservation Laws, *Phys. Rev. X* **8**, 021013 (2018).
- [21] S. Xu and B. Swingle, Locality, Quantum Fluctuations, and Scrambling, *Phys. Rev. X* **9**, 031048 (2019).
- [22] P. Zhang, Quantum chaos for the unitary Fermi gas from the generalized Boltzmann equations, *J. Phys. B: At. Mol. Opt. Phys.* **52**, 135301 (2019).
- [23] Y. Gu and A. Kitaev, On the relation between the magnitude and exponent of OTOCs, *J. High Energ. Phys.* **2019** (2), 75.
- [24] P. Zhang, Y. Gu, and A. Kitaev, An obstacle to sub-AdS holography for SYK-like models, *J. High Energ. Phys.* **2021** (3), 94.
- [25] H. Guo, Y. Gu, and S. Sachdev, Transport and chaos in lattice Sachdev-Ye-Kitaev models, *Phys. Rev. B* **100**, 045140 (2019).
- [26] A. Kitaev and S. J. Suh, The soft mode in the Sachdev-Ye-Kitaev model and its gravity dual, *J. High Energ. Phys.* **2018** (5), 183.
- [27] Y. Gu, A. Kitaev, and P. Zhang, A two-way approach to out-of-time-order correlators, *J. High Energ. Phys.* **2022** (3), 133.
- [28] J. Li, R. Fan, H. Wang, B. Ye, B. Zeng, H. Zhai, X. Peng, and J. Du, Measuring out-of-time-order correlators on a nuclear magnetic resonance quantum simulator, *Phys. Rev. X* **7**, 031011 (2017).
- [29] K. X. Wei, C. Ramanathan, and P. Cappellaro, Exploring localization in nuclear spin chains, *Phys. Rev. Lett.* **120**, 070501 (2018).
- [30] B. Foxen, C. Neill, A. Dunsworth, P. Roushan, B. Chiaro, A. Megrant, J. Kelly, Z. Chen, K. Satzinger, R. Barends, F. Arute, K. Arya, R. Babbush, D. Bacon, J. C. Bardin, S. Boixo, D. Buell, B. Burkett, Y. Chen, R. Collins, E. Farhi, A. Fowler, C. Gidney, M. Giustina, R. Graff, M. Harrigan, T. Huang, S. V. Isakov, E. Jeffrey, Z. Jiang, D. Kafri, K. Kechedzhi, P. Klimov, A. Korotkov, F. Kostriksa, D. Landhuis, E. Lucero, J. McClean, M. McEwen, X. Mi, M. Mohseni, J. Y. Mutus, O. Naaman, M. Neeley, M. Niu, A. Petukhov, C. Quintana, N. Rubin, D. Sank, V. Smelyanskiy, A. Vainsencher, T. C. White, Z. Yao, P. Yeh, A. Zalcman, H. Neven, and J. M. Martinis (Google AI Quantum), Demonstrating a continuous set of two-qubit gates for near-term quantum algorithms, *Phys. Rev. Lett.* **125**, 120504 (2020).
- [31] J. Braumüller, A. H. Karamlou, Y. Yanay, B. Kannan, D. Kim, M. Kjaergaard, A. Melville, B. M. Niedzielski, Y. Sung, A. Vepsäläinen, R. Winik, J. L. Yoder, T. P. Orlando, S. Gustavsson, C. Tahan, and W. D. Oliver, Probing quantum information propagation with out-of-time-ordered correlators, *Nature Physics* **18**, 172–178 (2021).
- [32] X. Mi, P. Roushan, C. Quintana, S. Mandrà, J. Marshall, C. Neill, F. Arute, K. Arya, J. Atalaya, R. Babbush, J. C. Bardin, R. Barends, J. Basso, A. Bengtsson, S. Boixo, A. Bourassa, M. Broughton, B. B. Buckley, D. A. Buell, B. Burkett, N. Bushnell, Z. Chen, B. Chiaro, R. Collins, W. Courtney, S. Demura, A. R. Derk, A. Dunsworth, D. Eppens, C. Erickson, E. Farhi, A. G. Fowler, B. Foxen, C. Gidney, M. Giustina, J. A. Gross, M. P. Harrigan, S. D. Harrington, J. Hilton, A. Ho, S. Hong, T. Huang, W. J. Huggins, L. B. Ioffe, S. V. Isakov, E. Jeffrey, Z. Jiang, C. Jones, D. Kafri, J. Kelly, S. Kim, A. Kitaev, P. V. Klimov, A. N. Ko-

- rotkov, F. Kostritsa, D. Landhuis, P. Laptev, E. Lucero, O. Martin, J. R. McClean, T. McCourt, M. McEwen, A. Megrant, K. C. Miao, M. Mohseni, S. Montazeri, W. Mruczkiewicz, J. Mutus, O. Naaman, M. Neeley, M. Newman, M. Y. Niu, T. E. O'Brien, A. Opremcak, E. Ostby, B. Pato, A. Petukhov, N. Redd, N. C. Rubin, D. Sank, K. J. Satzinger, V. Shvarts, D. Strain, M. Szalay, M. D. Trevithick, B. Villalonga, T. White, Z. J. Yao, P. Yeh, A. Zalcman, H. Neven, I. Aleiner, K. Kechedzhi, V. Smelyanskiy, and Y. Chen, Information scrambling in quantum circuits, *Science* **374**, 1479–1483 (2021).
- [33] M. Gärttner, J. G. Bohnet, A. Safavi-Naini, M. L. Wall, J. J. Bollinger, and A. M. Rey, Measuring out-of-time-order correlations and multiple quantum spectra in a trapped-ion quantum magnet, *Nature Physics* **13**, 781–786 (2017).
- [34] K. A. Landsman, C. Figgatt, T. Schuster, N. M. Linke, B. Yoshida, N. Y. Yao, and C. Monroe, Verified quantum information scrambling, *Nature* **567**, 61–65 (2019).
- [35] M. K. Joshi, A. Elben, B. Vermersch, T. Brydges, C. Maier, P. Zoller, R. Blatt, and C. F. Roos, Quantum information scrambling in a trapped-ion quantum simulator with tunable range interactions, *Physical Review Letters* **124**, 10.1103/physrevlett.124.240505 (2020).
- [36] S. Pegahan, I. Arakelyan, and J. Thomas, Energy-resolved information scrambling in energy-space lattices, *Physical Review Letters* **126**, 10.1103/physrevlett.126.070601 (2021).
- [37] A. Peres, Stability of quantum motion in chaotic and regular systems, *Phys. Rev. A* **30**, 1610 (1984).
- [38] H. Pastawski, P. Levstein, G. Usaj, J. Raya, and J. Hirschinger, A nuclear magnetic resonance answer to the boltzmann–loschmidt controversy?, *Physica A: Statistical Mechanics and its Applications* **283**, 166 (2000).
- [39] R. A. Jalabert and H. M. Pastawski, Environment-independent decoherence rate in classically chaotic systems, *Phys. Rev. Lett.* **86**, 2490 (2001).
- [40] T. Gorin, T. Prosen, T. H. Seligman, and M. Žnidarič, Dynamics of loschmidt echoes and fidelity decay, *Physics Reports* **435**, 33 (2006).
- [41] P. Jacquod and C. Petitjean, Decoherence, entanglement and irreversibility in quantum dynamical systems with few degrees of freedom, *Advances in Physics* **58**, 67 (2009).
- [42] A. Goussev, R. A. Jalabert, H. M. Pastawski, and D. A. Wisniacki, Loschmidt echo, *Scholarpedia* **7**, 11687 (2012).
- [43] E. L. Hahn, Spin echoes, *Phys. Rev.* **80**, 580 (1950).
- [44] W.-K. Rhim, A. Pines, and J. S. Waugh, Violation of the spin-temperature hypothesis, *Phys. Rev. Lett.* **25**, 218 (1970).
- [45] S. W. Morgan, V. Oganessian, and G. S. Boutis, Multi-spin correlations and pseudothermalization of the transient density matrix in solid-state nmr: Free induction decay and magic echo, *Phys. Rev. B* **86**, 214410 (2012).
- [46] S. Zhang, B. H. Meier, and R. R. Ernst, Polarization echoes in nmr, *Phys. Rev. Lett.* **69**, 2149 (1992).
- [47] P. R. Levstein, G. Usaj, and H. M. Pastawski, Attenuation of polarization echoes in nuclear magnetic resonance: A study of the emergence of dynamical irreversibility in many-body quantum systems, *The Journal of Chemical Physics* **108**, 2718 (1998).
- [48] C. M. Sánchez, A. K. Chattah, K. X. Wei, L. Buljubasich, P. Cappellaro, and H. M. Pastawski, Perturbation independent decay of the loschmidt echo in a many-body system, *Phys. Rev. Lett.* **124**, 030601 (2020).
- [49] C. M. Sánchez, A. K. Chattah, and H. M. Pastawski, Emergent decoherence induced by quantum chaos in a many-body system: A loschmidt echo observation through nmr, *Phys. Rev. A* **105**, 052232 (2022).
- [50] F. D. Domínguez, M. C. Rodríguez, R. Kaiser, D. Suter, and G. A. Álvarez, Decoherence scaling transition in the dynamics of quantum information scrambling, *Phys. Rev. A* **104**, 012402 (2021).
- [51] C. M. Sánchez, A. K. Chattah, K. X. Wei, L. Buljubasich, P. Cappellaro, and H. M. Pastawski, Perturbation independent decay of the loschmidt echo in a many-body system, *Physical review letters* **124**, 030601 (2020).
- [52] C. M. Sánchez, A. K. Chattah, and H. M. Pastawski, Emergent decoherence induced by quantum chaos in a many-body system: A loschmidt echo observation through nmr, *Physical Review A* **105**, 052232 (2022).
- [53] F. D. Domínguez, M. C. Rodríguez, R. Kaiser, D. Suter, and G. A. Álvarez, Decoherence scaling transition in the dynamics of quantum information scrambling, *Physical Review A* **104**, 012402 (2021).
- [54] J. Maldacena, S. H. Shenker, and D. Stanford, A bound on chaos, *Journal of High Energy Physics* **2016**, 10.1007/jhep08(2016)106 (2016).
- [55] R. Fan, P. Zhang, H. Shen, and H. Zhai, Out-of-Time-Order Correlation for Many-Body Localization, *Science Bulletin* **62**, 707 (2017).
- [56] B. Yan, L. Cincio, and W. H. Zurek, Information scrambling and loschmidt echo, *Phys. Rev. Lett.* **124**, 160603 (2020).
- [57] J. Kudler-Flam, L. Nie, and S. Ryu, Conformal field theory and the web of quantum chaos diagnostics, *Journal of High Energy Physics* **2020**, 10.1007/jhep01(2020)175 (2020).
- [58] Y.-L. Zhang, Y. Huang, and X. Chen, Information scrambling in chaotic systems with dissipation, *Physical Review B* **99**, 014303 (2019).
- [59] B. Yoshida and N. Y. Yao, Disentangling scrambling and decoherence via quantum teleportation, *Physical Review X* **9**, 011006 (2019).
- [60] Z. Xu, A. Chenu, T. Prosen, and A. del Campo, Thermofield dynamics: Quantum chaos versus decoherence, *Physical Review B* **103**, 064309 (2021).
- [61] Z. Xu, L. P. García-Pintos, A. Chenu, and A. Del Campo, Extreme decoherence and quantum chaos, *Physical Review Letters* **122**, 014103 (2019).
- [62] J. Tuziemski, Out-of-time-ordered correlation functions in open systems: A feynman-vernon influence functional approach, *Physical Review A* **100**, 062106 (2019).
- [63] S. Syzranov, A. Gorshkov, and V. Galitski, Out-of-time-order correlators in finite open systems, *Physical Review B* **97**, 161114 (2018).
- [64] P. Zanardi and N. Anand, Information scrambling and chaos in open quantum systems, *Physical Review A* **103**, 062214 (2021).
- [65] B. Swingle and N. Yunger Halpern, Resilience of scrambling measurements, *Physical Review A* **97**, 062113 (2018).
- [66] P. Zanardi and N. Anand, Information scrambling and chaos in open quantum systems, *Phys. Rev. A* **103**,

- 062214 (2021).
- [67] F. Arute, K. Arya, R. Babbush, D. Bacon, J. C. Bardin, R. Barends, R. Biswas, S. Boixo, F. G. Brandao, D. A. Buell, *et al.*, Quantum supremacy using a programmable superconducting processor, *Nature* **574**, 505 (2019).
- [68] J. R. González Alonso, N. Yunger Halpern, and J. Dressel, Out-of-time-ordered-correlator quasiprobabilities robustly witness scrambling, *Physical Review Letters* **122**, 040404 (2019).
- [69] B. Vermersch, A. Elben, L. M. Sieberer, N. Y. Yao, and P. Zoller, Probing scrambling using statistical correlations between randomized measurements, *Physical Review X* **9**, 021061 (2019).
- [70] K. Agarwal and N. Bao, Toy model for decoherence in the black hole information problem, *Physical Review D* **102**, 086017 (2020).
- [71] A. Touil and S. Deffner, Information scrambling versus decoherence—two competing sinks for entropy, *PRX Quantum* **2**, 010306 (2021).
- [72] F. Andreadakis, N. Anand, and P. Zanardi, Scrambling of algebras in open quantum systems, *Physical Review A* **107**, 042217 (2023).
- [73] J. Harris, B. Yan, and N. A. Sinitsyn, Benchmarking information scrambling, *Physical Review Letters* **129**, 050602 (2022).
- [74] Y.-N. Zhou, L. Mao, and H. Zhai, Rényi entropy dynamics and lindblad spectrum for open quantum systems, *Phys. Rev. Res.* **3**, 043060 (2021).
- [75] Y.-N. Zhou, Generalized Lindblad master equation for measurement-induced phase transition, *SciPost Physics Core* **6**, 023 (2023).
- [76] J. Glatthard, Page-curve-like entanglement dynamics in open quantum systems, *Phys. Rev. D* **109**, L081901 (2024).
- [77] K. Kobayashi, [Time evolution of the von neumann entropy in open quantum system](#) (2024), [arXiv:2405.11824 \[quant-ph\]](#).
- [78] A. Bhattacharya, P. Nandy, P. P. Nath, and H. Sahu, Operator growth and Krylov construction in dissipative open quantum systems, *J. High Energ. Phys.* **2022** (12), 1.
- [79] T. Schuster and N. Y. Yao, Operator growth in open quantum systems, *Phys. Rev. Lett.* **131**, 160402 (2023).
- [80] C. Liu, H. Tang, and H. Zhai, Krylov complexity in open quantum systems, *Phys. Rev. Res.* **5**, 033085 (2023).
- [81] B. Bhattacharjee, X. Cao, P. Nandy, and T. Pathak, Operator growth in open quantum systems: Lessons from the dissipative SYK, *J. High Energ. Phys.* **2023** (3), 54.
- [82] A. Bhattacharya, P. Nandy, P. P. Nath, and H. Sahu, On krylov complexity in open systems: an approach via bi-lanczos algorithm, *Journal of High Energy Physics* **2023**, 10.1007/jhep12(2023)066 (2023).
- [83] R. Ma, J.-H. Zhang, Z. Bi, M. Cheng, and C. Wang, [Topological phases with average symmetries: the decohered, the disordered, and the intrinsic](#) (2024), [arXiv:2305.16399 \[cond-mat.str-el\]](#).
- [84] L. A. Lessa, R. Ma, J.-H. Zhang, Z. Bi, M. Cheng, and C. Wang, [Strong-to-weak spontaneous symmetry breaking in mixed quantum states](#) (2024), [arXiv:2405.03639 \[quant-ph\]](#).
- [85] P. Sala, S. Gopalakrishnan, M. Oshikawa, and Y. You, [Spontaneous strong symmetry breaking in open systems: Purification perspective](#) (2024), [arXiv:2405.02402 \[quant-ph\]](#).
- [86] Y. Xu and C.-M. Jian, [Average-exact mixed anomalies and compatible phases](#) (2024), [arXiv:2406.07417 \[cond-mat.str-el\]](#).
- [87] X. Huang, M. Qi, J.-H. Zhang, and A. Lucas, [Hydrodynamics as the effective field theory of strong-to-weak spontaneous symmetry breaking](#) (2024), [arXiv:2407.08760 \[cond-mat.str-el\]](#).
- [88] Y. Kuno, T. Orito, and I. Ichinose, Strong-to-weak symmetry breaking states in stochastic dephasing stabilizer circuits, *Physical Review B* **110**, 10.1103/physrevb.110.094106 (2024).
- [89] M. M. Taddei, B. M. Escher, L. Davidovich, and R. L. de Matos Filho, Quantum speed limit for physical processes, *Phys. Rev. Lett.* **110**, 050402 (2013).
- [90] A. del Campo, I. L. Egusquiza, M. B. Plenio, and S. F. Huelga, Quantum speed limits in open system dynamics, *Phys. Rev. Lett.* **110**, 050403 (2013).
- [91] S. Deffner and E. Lutz, Quantum speed limit for non-markovian dynamics, *Physical Review Letters* **111**, 10.1103/physrevlett.111.010402 (2013).
- [92] L. P. García-Pintos, S. B. Nicholson, J. R. Green, A. del Campo, and A. V. Gorshkov, Unifying quantum and classical speed limits on observables, *Phys. Rev. X* **12**, 011038 (2022).
- [93] S. Nakajima and Y. Utsumi, Speed limits of the trace distance for open quantum system, *New Journal of Physics* **24**, 095004 (2022).
- [94] K. Sekiguchi, S. Nakajima, K. Funo, and H. Tajima, [Improvement of speed limits: Quantum effect on the speed in open quantum systems](#) (2024), [arXiv:2410.11604 \[quant-ph\]](#).
- [95] Y.-N. Zhou, X. Li, H. Zhai, C. Li, and Y. Gu, Reviving the lieb–schultz–mattis theorem in open quantum systems, *National Science Review* , nwae287 (2024).
- [96] K. Kawabata, R. Sohal, and S. Ryu, Lieb-schultz-mattis theorem in open quantum systems, *Physical Review Letters* **132**, 10.1103/physrevlett.132.070402 (2024).
- [97] J. E. Tyson, Operator-schmidt decompositions and the fourier transform, with applications to the operator-schmidt numbers of unitaries, *Journal of Physics A: Mathematical and General* **36**, 10101–10114 (2003).
- [98] M. Zwolak and G. Vidal, Mixed-state dynamics in one-dimensional quantum lattice systems: A time-dependent superoperator renormalization algorithm, *Physical Review Letters* **93**, 10.1103/physrevlett.93.207205 (2004).
- [99] T. Prosen, Third quantization: a general method to solve master equations for quadratic open fermi systems, *New Journal of Physics* **10**, 043026 (2008).
- [100] L. Mandelstam and I. G. Tamm, The Uncertainty Relation Between Energy and Time in Non-relativistic Quantum Mechanics, in *Selected Papers*, edited by I. E. Tamm, B. M. Bolotovskii, V. Y. Frenkel, and R. Peierls (Springer, Berlin, Heidelberg, 1991) pp. 115–123.
- [101] N. Margolus and L. B. Levitin, The maximum speed of dynamical evolution, *Physica D: Nonlinear Phenomena* **120**, 188–195 (1998).
- [102] L. B. Levitin and T. Toffoli, Fundamental limit on the rate of quantum dynamics: The unified bound is tight, *Phys. Rev. Lett.* **103**, 160502 (2009).
- [103] M. R. Frey, Quantum speed limits—primer, perspectives, and potential future directions, *Quantum Inf Process* **15**, 3919 (2016).

- [104] S. Deffner and S. Campbell, Quantum speed limits: from heisenberg’s uncertainty principle to optimal quantum control, *Journal of Physics A: Mathematical and Theoretical* **50**, 453001 (2017).
- [105] S. Sachdev and J. Ye, Gapless spin-fluid ground state in a random quantum heisenberg magnet, *Physical Review Letters* **70**, 3339–3342 (1993).
- [106] A. Kitaev, [A simple model of quantum holography \(part 1\)](#), Kavli Institute for Theoretical Physics Program: Entanglement in Strongly-Correlated Quantum Matter (Apr 6 - Jul 2, 2015). (2015).
- [107] S. Sachdev, Bekenstein-Hawking Entropy and Strange Metals, *Phys. Rev. X* **5**, 041025 (2015).
- [108] J. Maldacena and D. Stanford, Remarks on the Sachdev-Ye-Kitaev model, *Phys. Rev. D* **94**, 106002 (2016).
- [109] A. Kulkarni, T. Numasawa, and S. Ryu, Lindbladian dynamics of the sachdev-ye-kitaev model, *Physical Review B* **106**, 075138 (2022).
- [110] The imaginary part of the Lindblad spectrum determines the decay of the double space wavefunction. The modulus of the double space wavefunction is related to the second Renyi entropy by the equation $e^{-S^{(2)}} = \text{Tr}[\rho^2] = \langle \psi_\rho | \psi_\rho \rangle$. Therefore, the decay of the modulus of the double space wavefunction corresponds to the growth of the second Renyi entropy. In the weak dissipation limit, the imaginary part of the Lindblad spectrum is of order γ . Consequently, in this limit, the dynamics of the second Renyi entropy satisfy a γt scale.
- [111] W. H. Zurek, Decoherence, einselection, and the quantum origins of the classical, *Reviews of modern physics* **75**, 715 (2003).
- [112] D. Schlosshauer, the quantum-to-classical transition, *The Frontiers Collection* (Springer-Verlag, 2007) (2007).
- [113] The logic here is that the reduced evolution of R_B can be viewed as a general open system dynamics. Under the Born-Markov approximation, this open-system evolution can be expressed in the form of a Lindblad master equation, where the Lindblad jump operators are determined by the interaction between the system and the bath. The Lindblad evolution can equivalently be described as the system’s evolution under an effective Hamiltonian with random noise. The average of this random noise, referred to as Langevin noise in the literature, must satisfy certain properties.
- [114] In the appendix, we provide the proof of the OTOC-LE relation in closed systems (A) and open systems (B) using the diagrammatic representation.
- [115] F. Schwarz, M. Goldstein, A. Dorda, E. Arrigoni, A. Weichselbaum, and J. von Delft, Lindblad-driven discretized leads for nonequilibrium steady-state transport in quantum impurity models: Recovering the continuum limit, *Physical Review B* **94**, 155142 (2016).
- [116] Here, we consider local dissipation, which does not involve interactions between subsystems A and B. Therefore, we use the same approximation as in the proof of the OTOC-LE relation for closed systems, where the effect of coupling on the reduced evolution of the operator R_B is approximated as random noise on subsystem B.
- [117] S. A. Weidinger, M. Heyl, A. Silva, and M. Knap, Dynamical quantum phase transitions in systems with continuous symmetry breaking, *Physical Review B* **96**, 10.1103/physrevb.96.134313 (2017).
- [118] S. Lieu, M. McGinley, and N. R. Cooper, Tenfold way for quadratic lindbladians, *Phys. Rev. Lett.* **124**, 040401 (2020).
- [119] L. Sá, P. Ribeiro, and T. c. v. Prosen, Symmetry classification of many-body lindbladians: Tenfold way and beyond, *Phys. Rev. X* **13**, 031019 (2023).
- [120] K. Kawabata, A. Kulkarni, J. Li, T. Numasawa, and S. Ryu, Symmetry of open quantum systems: Classification of dissipative quantum chaos, *PRX Quantum* **4**, 030328 (2023).
- [121] L. Mao, F. Yang, and H. Zhai, Symmetry-preserving quadratic lindbladian and dissipation driven topological transitions in gaussian states, *Reports on Progress in Physics* **87**, 070501 (2024).

Appendix A: The diagrammatic proof of the OTOC-LE relation in closed system

We provide a diagrammatic proof of the OTOC-LE relation (the similar diagrammatic proof technique can be found in [55]), as reviewed in the Section IV of the main text.

For a general operator Q , if we choose a complete orthogonal basis of subsystems A and B, we can write it as

$$Q = \sum_{i_A, i_B, j_A, j_B} Q_{i_A, i_B, j_A, j_B} |i_A\rangle |i_B\rangle \langle j_A| \langle j_B|. \quad (\text{A1})$$

The diagram illustrating this is shown in Fig. 5(a), where the left legs represent the input and the right legs represent the output. When we perform a partial trace over the degrees of freedom of subsystem B, in the diagram, this involves connecting the input and output legs of subsystem B, as depicted in Fig. 5(b).

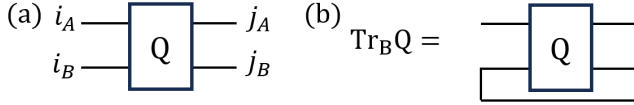


FIG. 5. The diagram represents the general operator Q in (a) and the partial trace over subsystem B of it in (b).

We will then use this diagrammatic technique to prove the OTOC-LE relation. For simplicity, we consider the infinite-temperature case, where $\rho(0) \propto \mathcal{I}$.

First, we can present the OTOC defined as

$$F_{\beta=0}(t) = \text{Tr}[R_B^\dagger(t) W_A^\dagger R_B(t) W_A] \quad (\text{A2})$$

in the Fig. 6.

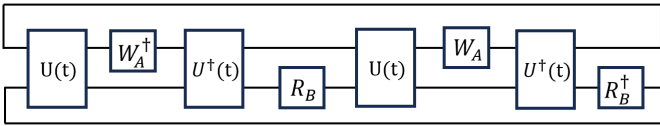


FIG. 6. The diagram representation of OTOC is defined in the Eq. (A2).

Next, we perform the random averaging over operators on subsystem A

$$\overline{F(t)} = \frac{1}{d_A} \int dW_A \text{Tr} [R_B^\dagger(t) W_A^\dagger R_B(t) W_A]. \quad (\text{A3})$$

We use the Harr random average formula,

$$\int dW_A W_A^\dagger O W_A = \frac{1}{d_A} \mathcal{I}_A \otimes \text{Tr}_A(O), \quad (\text{A4})$$

and it is depicted as the Fig. 7 (the constant $\frac{1}{d_A}$ has been omitted).

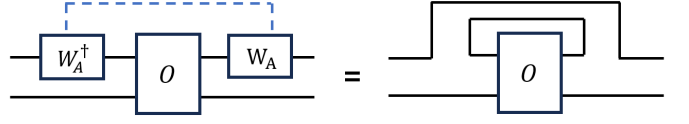


FIG. 7. The diagram representation of the Harr random average formula Eq. (A4). The blue dash line represents the Harr random average of the operator W_A defined on subsystem A.

The diagrammatic representation of the average OTOC in Eq. (A3) is shown in Fig. 8 where the blue dash line represents the Harr random average of the operator W_A .

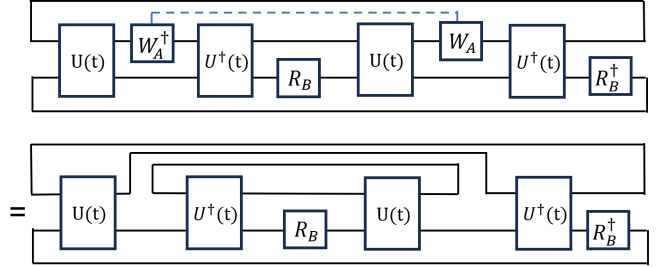


FIG. 8. The diagram representation of the average of OTOC over W_A .

To account for the effect of the coupling on the reduced evolution of the operator R_B , we approximately treat it as random noises acting on subsystem B,

$$\text{Tr}_A(e^{iHt} R_B e^{-iHt}) \simeq d_A \overline{e^{i(H_B + V_\alpha)t} R_B e^{-i(H_B + V_\alpha)t}}. \quad (\text{A5})$$

The logic here is that the reduced evolution of R_B can be viewed as a general open system dynamics where the open system (subsystem B) evolves together with the bath (subsystem A) unitarily. We consider the open system dynamics by tracing out the bath degree of freedom. Under the Born-Markov approximation, the open system evolution can be written as the form of the Lindblad master equation, where the form of the Lindblad jump operators is decided by the interaction between the system and the bath. The Lindblad evolution can be equivalently written as the system evolution under the effective Hamiltonian with random noise, this random noise has to satisfy some average properties, and this noise is called Langevin noise in literature.

The diagrammatic representation of this approximation is shown in Fig. 9, where the orange dotted line represents the random averaging over the noises $\{V_\alpha\}$. Incorporating this diagram into the averaged OTOC, we obtain the diagram shown in Fig. 10.

Next, we consider the averaging of operators on subsystem B, with the diagrammatic representation shown in Fig. 11. Note that the final line in Fig. 11 takes the form of the LE. Through these procedures, we have shown that the averaged OTOC in Eq. (15) can be further expressed

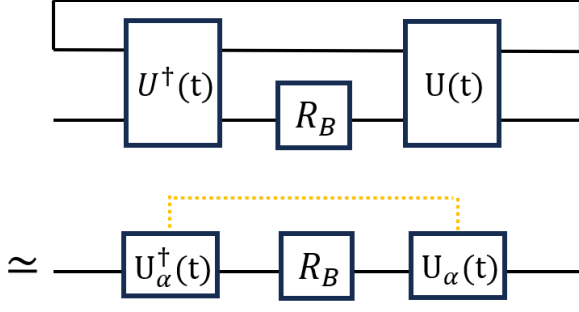


FIG. 9. The diagram representation of reduced evolution of R_B . Here, the effect of coupling on the reduced evolution of the operator R_B is approximated as random noise $\{V_\alpha\}$ on subsystem B, and the orange dot line denotes the random average over noise $\{V_\alpha\}$.

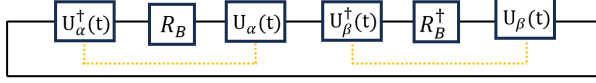


FIG. 10. The diagram representation of the average of OTOC over W_A after using the approximation of Fig. 9. Here, the orange dot line denotes the random average over noise on the subsystem B.

as

$$\overline{F(t)} \simeq \frac{1}{d_B^2} |\text{Tr}_B [e^{-i(H_B+V_\alpha)t} e^{i(H_B+V_\beta)t}]|^2. \quad (\text{A6})$$

Recall that the definition of the LE at infinite temperature is

$$M(t) = |\text{Tr}[e^{iH_1 t} e^{-iH_2 t}]|^2. \quad (\text{A7})$$

We then observe that the final line of Fig. 11 takes the form of the LE.

Appendix B: The diagrammatic proof of the OTOC-LE relation in open system

Below, we provide a diagrammatic proof of the OTOC-LE relation for open systems, which is quite similar to the proof for closed systems, except that the evolution is now governed by Lindblad dynamics rather than unitary evolution. For simplicity, we consider the infinite temperature case, where $\rho(0) \propto \mathcal{I}$. and we assume the Lindblad jump operators are all hermitian, thus $\tilde{\mathcal{L}}^\dagger = \mathcal{L}$ (the definition of $\tilde{\mathcal{L}}$ denote the backward Lindblad evolution and \mathcal{L}^\dagger denote the adjoint Lindblad evolution, their definition are in the Eq. (23) and Eq. (24) respectively).

The average OTOC over the random unitary operator

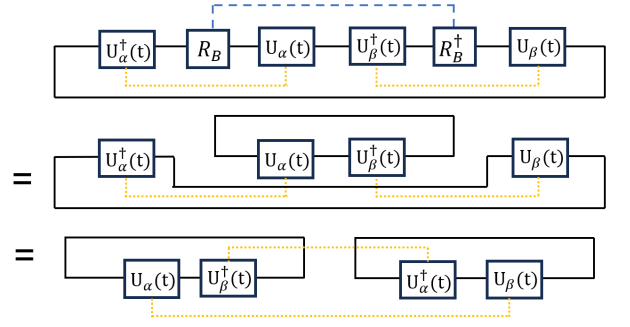


FIG. 11. The diagram representation of OTOC averaged over the random unitary operator on subsystems A and B. Here, the blue dash line represents the random average over the unitary operators R_B , and the orange dot lines denote the random average over noise on subsystem B.

W_A defined on subsystem A

$$\int dW_A F^D(t) = \frac{1}{d_A} \int dW_A \text{Tr}\{R_B^\dagger e^{\mathcal{L}^\dagger t} [W_A^\dagger e^{\mathcal{L} t} [R_B] W_A]\}. \quad (\text{B1})$$

is represented in Fig. 12.

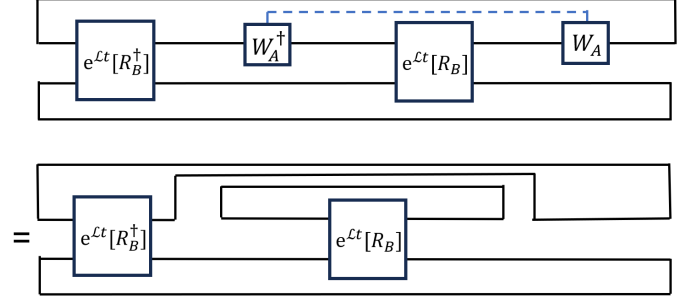


FIG. 12. The diagram representation of the average OTOC of operator W_A supported on the subsystem A.

Here, we consider local dissipation, which does not involve interactions between subsystems A and B. Therefore, we use the same approximation as in the proof of the OTOC-LE relation for closed systems, where the effect of coupling on the reduced evolution of the operator R_B is approximated as random noise on subsystem B. This approximation can be generally formulated as

$$\text{Tr}_A [e^{\mathcal{L} t} [R_B]] \simeq d_A \overline{e^{\mathcal{L}_{B,\alpha t}} [R_B]},$$

and it is shown as Fig. 13.

Incorporating this diagram into the averaged OTOC, we obtain the diagram shown in Fig. 14, where we omit the subscript B.

Then, we do the average over R_B . We have shown it in the Fig. 15. We have decomposed the Lindblad evolu-

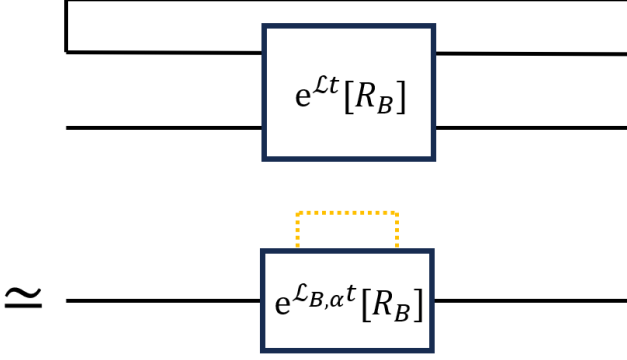


FIG. 13. The diagram representation of reduced evolution of R_B in open system. Here, the effect of coupling on the reduced evolution of the operator R_B is approximated as random noise $\{V_\alpha\}$ on subsystem B, and the orange dot line denotes the random average over noise $\{V_\alpha\}$.

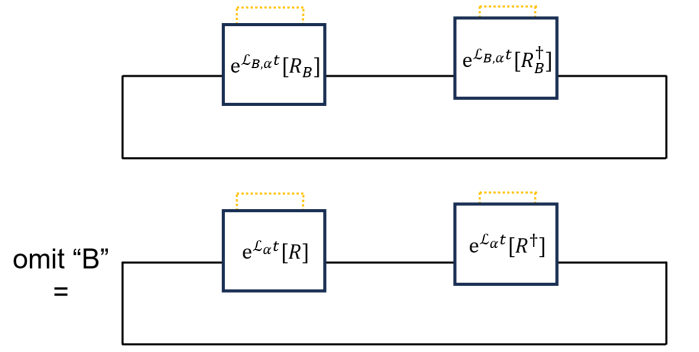


FIG. 14. The diagram representation of the average of OTOC after averaging over operators on subsystem A. We have omitted the subscript B since both the time evolution and operators only non-trivially act on subsystem B.

tion into two blocks, denoted as \mathcal{L}^F and \mathcal{L}^B (to facilitate comparison with the unitary evolution in closed systems, we use F to denote *forward* and B to denote *backward*). The black dashed-dot line indicates that there are correlations between the F and B blocks in the Lindblad evolution.

Examining the last line of Fig. 15, we find that it takes the form of the unnormalized LE in the open system.

$$\overline{F^D}(t) = \frac{1}{d_B^2} \text{Tr}_B \left[e^{i(H_B^{D\dagger} + V_\alpha^\dagger)t} e^{-i(H_B^D + V_\beta)t} \right]. \quad (\text{B2})$$

where the forward and backward lindblad evolutions are represented as \mathcal{L}_α and \mathcal{L}_β . Additionally, when we replace the Lindblad evolution with the unitary evolution of the closed system, we find that this diagram reverts to the form of the LE for the closed system, as depicted in the last line of Fig. 11.

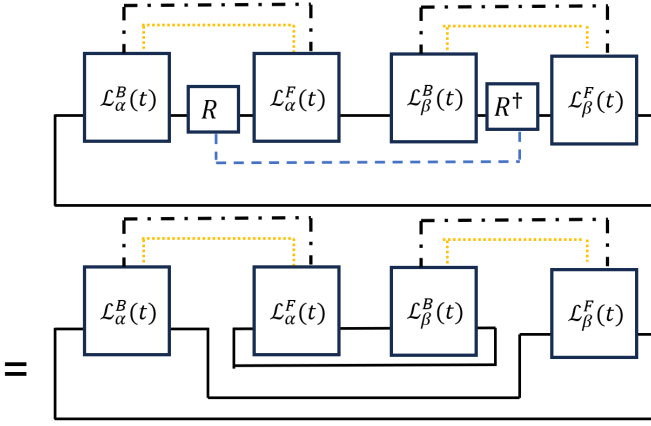


FIG. 15. The diagram representation of the average of OTOC over operator R . The black dashed-dot line indicates the correlations between the forward(F) and backward(B) blocks of the Lindblad evolution.